

## Rice Husk Reuse in the Preparation of SnO<sub>2</sub>/SiO<sub>2</sub> Nanocomposite

Carlos Sérgio Ferreira<sup>a</sup>, Pâmyla Layene Santos<sup>b</sup>, Juliano Alves Bonacin<sup>b</sup>, Raimundo Ribeiro Passos<sup>a</sup>,

Leandro Aparecido Pocrifka<sup>a\*</sup>

<sup>a</sup>GEMATA - LEEN, Departamento de Química, Universidade Federal do Amazonas – UFAM, CEP 69077-000, Manaus, AM, Brazil

<sup>b</sup>Molecular Nanotechnology Laboratory - LNaNOMOL, Instituto de Química, Universidade Estadual de Campinas – UNICAMP, CP 6154, CEP 13083-970, Campinas, SP, Brazil

Received: April 22, 2015; Revised: June 9, 2015

In this study, biogenic SiO<sub>2</sub> of high purity and high surface area obtained from rice husk was used for prepare a nanostructured SnO<sub>2</sub>/SiO<sub>2</sub> composite. The predominantly amorphous silica was extracted in an acidic route and then the nanocomposite was done via sol-gel route using ethylene glycol and citric acid followed by heat treatment. SiO<sub>2</sub> content of the rice husk was determined by X-ray fluorescence (XRF) and its specific surface area determined by nitrogen adsorption. The composite nanostructured SnO<sub>2</sub>/SiO<sub>2</sub> was structurally characterized by the techniques of X-ray diffraction (XRD), Raman and Fourier transform infrared (FT-IR) spectroscopy. The morphological characteristics were revealed by scanning electron microscope (SEM).

**Keywords:** *biogenic SiO<sub>2</sub>, rice husk, SnO<sub>2</sub>/SiO<sub>2</sub> composite, Pechini method*

### 1. Introduction

Agroindustry has generated a large content of residues and a necessity of utilization of these residues might reduce pollution and increase energy savings. Among these residues, rice husks have received attention due to its large volume produced and high content of amorphous silica, approximately 21%<sup>1,2</sup>. SiO<sub>2</sub> can be obtained by direct calcination followed by calcination chemical treatment, and by sol-gel route. Silica from rice husk is considered as an alternative to commercial silica<sup>3</sup> due to low cost and wide application, such as to obtain silicon carbide<sup>4</sup>, catalysts<sup>5</sup>, adsorbents<sup>6</sup>, zeolites<sup>7</sup>, silicates<sup>8</sup> and cement<sup>9</sup>.

Compared to conventional materials, nanomaterials have interesting physical and chemical properties, besides several areas of application, and relative easy production carried out by different methods such as microemulsion<sup>10</sup>, hydrothermal<sup>11</sup> and sol-gel<sup>12</sup>.

Tin oxide (SnO<sub>2</sub>) is an important semiconductor oxide in the industry<sup>13</sup>, but despite its wide usage<sup>14-17</sup> has low thermal stability and tendency to aggregation<sup>18</sup>, that can be overcome by incorporating the amorphous SiO<sub>2</sub> to SnO<sub>2</sub><sup>19</sup>, generating the SnO<sub>2</sub>/SiO<sub>2</sub> nanocomposite. There are several studies using SnO<sub>2</sub>/SiO<sub>2</sub>, like composite<sup>20</sup>, xerogel<sup>21</sup>, nanotubes<sup>22</sup> and films<sup>23</sup>, which application can be in photocatalysis<sup>24</sup> and sensors<sup>25</sup>.

This work aims prepare and characterize SnO<sub>2</sub>/SiO<sub>2</sub> nanocomposites from amorphous biogenic silica of high purity extracted from rice husk by Pechini method<sup>26</sup>, as an alternative to TEOS (tetraethoxysilane). Silica from rice husk was characterized by X-ray fluorescence (XRF) and by physical adsorption of nitrogen. The SnO<sub>2</sub>/SiO<sub>2</sub> nanocomposite was characterized by scanning electron microscopy (SEM), by

X-ray diffractometry (XRD) and Raman spectroscopy and Fourier transform infrared spectroscopy (FT-IR).

### 2. Experimental

#### 2.1. Extraction of SiO<sub>2</sub> and Preparations of nanocomposite

Extraction of silica was made by grinding of the rice husk (RH) followed by chemical treatment with HCl (10% v/v), in the ratio RH:HCl 1:3, for one hour with constant stirring to solubilize organic matter. The solubilized RH was washed with ultrapure water and it was filtered under vacuum, obtaining a pulp (PRH) which was treated with a solution of H<sub>2</sub>SO<sub>4</sub> and H<sub>2</sub>O<sub>2</sub> in the ratio of 1:2:1 (w/v/v) - PRH:H<sub>2</sub>SO<sub>4</sub>:H<sub>2</sub>O<sub>2</sub> - under constant stirring for one hour to promote the oxidation of organic matter. Finally, the oxidized PRH was washed with ultrapure water and the biogenic SiO<sub>2</sub> was obtained by vacuum filtering and calcinations in an oven for 4h at 600 °C.

SnO<sub>2</sub>/SiO<sub>2</sub> nanocomposite was prepared by adding biogenic silica and SnCl<sub>2</sub>·2H<sub>2</sub>O to a solution of nitric acid (NA)/ethylene glycol (EG), obeying the following proportions 1:3:12 (SnCl<sub>2</sub>·2H<sub>2</sub>O: CA: EG) and 1:4 (w / w) - (SiO<sub>2</sub>: SnCl<sub>2</sub>·2H<sub>2</sub>O). This mixture was stirred for 1h at 60 °C with subsequent heat treatment at 250 °C for 2 hours, followed by calcination at 400 °C during 1 hour. All steps of calcination and heat treatment were performed without heating rate.

#### 2.2. Characterization

Biogenic silica was characterized by x-ray fluorescence (XRF) using an Epsilon 3XL spectrometer. Specific surface area was determined by nitrogen gas adsorption using a

\*e-mail: [pocrifka@gmail.com](mailto:pocrifka@gmail.com)

Quantachrome Autosorb-iQ equipment by multipoint BET method (Brunauer Emmett Tell) and the average diameter of the silica particles was estimated using the following equation for spherical particles

$$d_{BET} = \frac{6}{(A_{BET} \cdot \rho_{TEO})} \quad (1)$$

where  $\rho_{TEO}$  is the theoretical density<sup>27</sup> for the amorphous silica, having a value of 1,92 g cm<sup>-3</sup> and  $A_{BET}$  is the specific surface area.

Morphology of SnO<sub>2</sub>/SiO<sub>2</sub> nanocomposite was determined by scanning electron microscopy (SEM) using a JEOL model JMS6360-Lv microscope. The crystallinity of the material were characterized by X-ray diffraction (Shimadzu/XRD-7000) with CuK $\alpha$  radiation ( $\lambda = 1.542\text{\AA}$ ), 40 kV and 30 mA. Vibrational spectra were recorded on a Bomem MB-series spectrophotometer (Model B100) and Raman spectra were obtained using Confocal Raman equipment model T64000 Jobin-Yvon with laser excitation at 532 nm. Composition of the biogenic silica and the nanocomposite were identified by XRF, and the crystallite size was determined by Debye-Scherrer equation:

$$d = \frac{K\lambda}{\beta \cos\theta} \quad (2)$$

where  $d$  is crystallite size,  $K$  is shape factor (typical value of about 0.89 for spherical crystalline solids with cubic unit cells),  $\lambda$  is CuX-ray wavelength (1.542 Å),  $\theta$  is Bragg diffraction angle and  $\beta$  is the peak width of the diffraction peak profile at half maximum height.

## 3. Results and Discussion

### 3.1. Amorphous SiO<sub>2</sub>

Composition of the biogenic silica is shown in Table 1. According to the percentage values of the components, the methodology used to extraction provided SiO<sub>2</sub> with purity of approximately 98.6%, higher than commercial SiO<sub>2</sub><sup>[28]</sup>. The analysis of the surface area by BET method showed an approximated<sup>29,30</sup> value of 450 m<sup>2</sup> g<sup>-1</sup> and a mean particle size of 7 nm, given by Equation 1.

### 3.2. Structural study of SiO<sub>2</sub> and nanocomposite

XRD diffractogram of the biogenic SiO<sub>2</sub> is presented in Figure 1a and shows a broad peak located approximately at  $2\theta = 22.5^\circ$ , that suggests an amorphous characteristic of

**Table 1.** Composition of SiO<sub>2</sub> determined by XRF.

Component	%
SiO <sub>2</sub>	98.589
P <sub>2</sub> O <sub>5</sub>	0.834
Al <sub>2</sub> O <sub>3</sub>	0.390
CaO	0.130
Fe <sub>2</sub> O <sub>3</sub>	0.020
Ag <sub>2</sub> O	0.011
MnO	0.007
TiO <sub>2</sub>	0.003
Cl	0.016

the sample and agrees with the reported JCPDS data (card No. 01-086-1561).

XRD pattern for the nanocomposite is shown in Figure 1b and reveals a small shoulder at  $2\theta = 21.7^\circ$  that can be attributed to amorphous SiO<sub>2</sub> and other peaks assigned to crystalline SnO<sub>2</sub>. All values of diffraction peaks are in accordance with JCPDS pattern (card No. 00-041-1485). The main diffraction peaks observed for SnO<sub>2</sub> are centered approximately at  $2\theta$  values of 27.1°, 34.2° and 52.1°. In addition, the crystallite size based on the major diffraction peak is 27.8 nm for the nanocomposite.

### 3.3. Morphology of nanocomposite

Surface morphology of the nanocomposite is presented in Figure 2. SEM micrographs reveal formation of a heterogeneous mixture of agglomerates with irregular shapes and sizes.

### 3.4. FTIR and Raman analyses

FT-IR and Raman spectra for the SnO<sub>2</sub>/SiO<sub>2</sub> nanocomposite are shown in Figure 3a and 3b, respectively. Comparisons between wavenumber obtained in this work with literature values are exhibited in Tables 2 and 3.

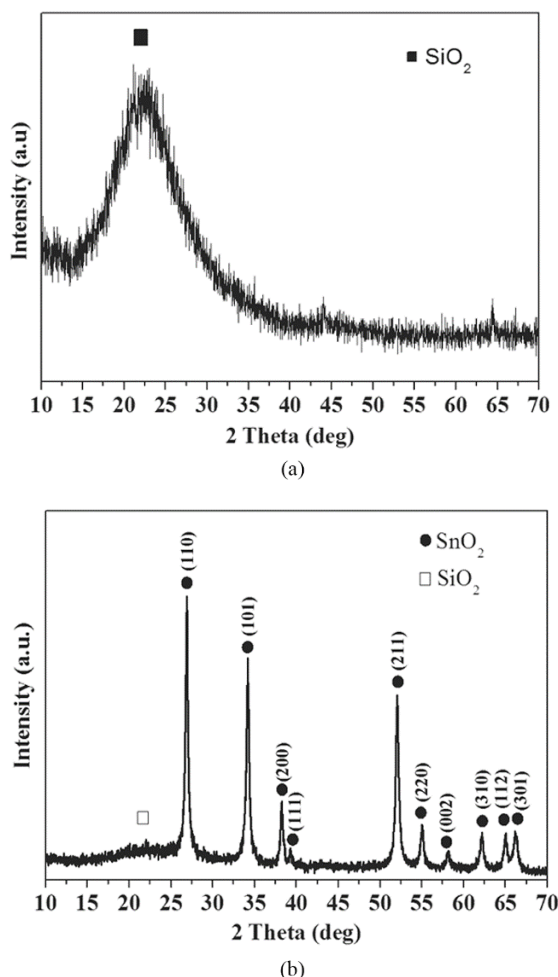


**Figure 1.** XRD obtained for (a) biogenic SiO<sub>2</sub> from rice husk and (b) SnO<sub>2</sub>/SiO<sub>2</sub> nanocomposite.

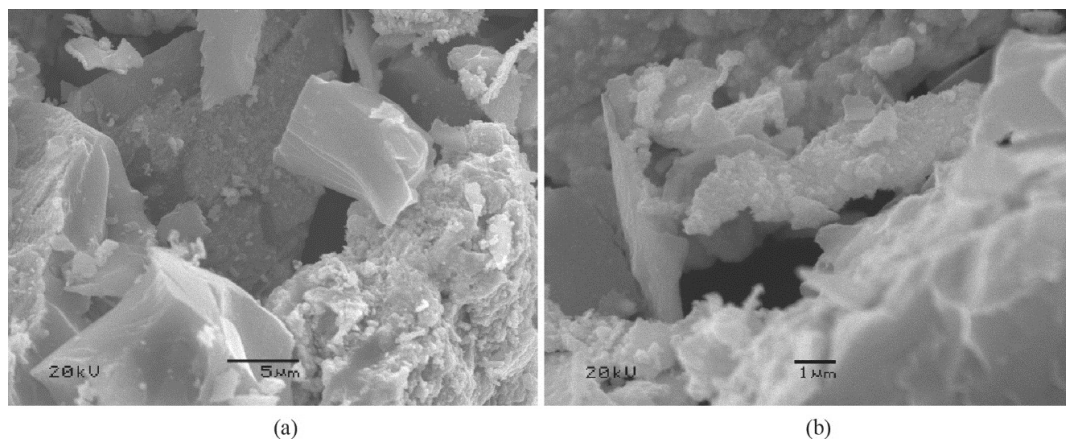


Figure 2. SEM images magnified (a) 3500 and (b) 10000 times.

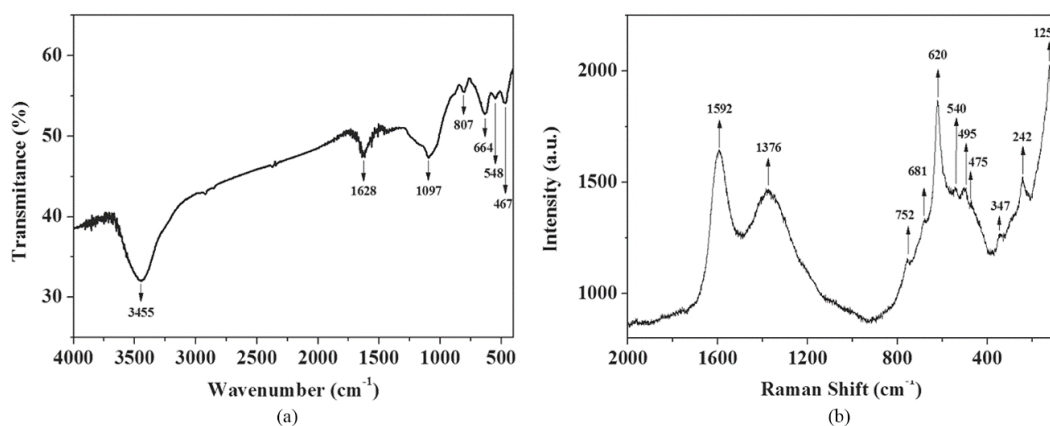


Figure 3. Spectra for the SnO<sub>2</sub>/SiO<sub>2</sub> nanocomposite (a) FT-IR (b) Raman.

Table 2. Assignments of infrared bands of the SnO<sub>2</sub>/SiO<sub>2</sub> nanocomposite.

This work (cm <sup>-1</sup> )	Literature <sup>Ref</sup> (cm <sup>-1</sup> )	Assignment
467	460 <sup>30</sup>	δ (Si-O)
548	558 <sup>32</sup>	$\nu_{\text{sim}}$ (Sn-O)
664	674 <sup>32</sup>	$\nu_{\text{ass}}$ (Sn-O-Sn)
807	800 <sup>30</sup>	$\nu_{\text{sim}}$ (Si-O-Si)
1097	1074 <sup>30</sup>	$\nu_{\text{ass}}$ (Si-O-Si)
1628	1620-1630 <sup>29</sup>	δ (H-O-H)
3455	3350-3450 <sup>29</sup>	$\nu$ (O-H)

Infrared spectrum shows a broad band at 3455 cm<sup>-1</sup> attributed to O-H stretching from hydroxyl groups presents on surface of the material and the band at 1628 cm<sup>-1</sup> is associated with bending H-O-H bond groups of adsorbed water molecules<sup>31</sup>. Bands at 467, 807 and 1097 cm<sup>-1</sup> are assigned respectively to vibrational modes of O-Si-O bending, to symmetric stretching of Si-O-Si group and to the asymmetric stretching of Si-O-Si structural bond of siloxane<sup>32</sup>. Vibrations in the range from 500 to 700 cm<sup>-1</sup> are assigned to Sn-O-Sn group as result of condensation reactions<sup>33</sup>. The bands characterized by the peaks 548 and 664 cm<sup>-1</sup> are assigned to the Sn-O stretching vibration and Sn-O-Sn asymmetric vibration, respectively<sup>34</sup>.

Table 3. Assignments of the Raman bands for the SnO<sub>2</sub>/SiO<sub>2</sub> nanocomposite.

This work (cm <sup>-1</sup> )	Literature <sup>Ref</sup> (cm <sup>-1</sup> )	Assignment
1592	1580 <sup>40</sup>	G band
1376	1360 <sup>40</sup>	D band
752	774 <sup>34</sup> , 775 <sup>35</sup>	B <sub>2g</sub>
681	687 <sup>34</sup>	A <sub>2u</sub> LO*
620	638 <sup>34</sup> , 631 <sup>35</sup>	A <sub>1g</sub>
540	512 <sup>34</sup>	A <sub>2u</sub> TO†
495	475 <sup>34</sup> , 474 <sup>35</sup>	E <sub>g</sub>
347	377 <sup>34</sup>	E <sub>u</sub> (2) LO
242	236 <sup>34</sup>	E <sub>u</sub> (1) TO
125	100 <sup>34</sup>	B <sub>1g</sub>

\*LO – longitudinal optical phonons. †TO – transverse optical phonons.

SnO<sub>2</sub> has a tetragonal rutile crystalline structure with point group D<sub>4h</sub><sup>35</sup>. According to Li *et al.* there are three typical modes to SnO<sub>2</sub> in Raman spectrum (474 cm<sup>-1</sup> (E<sub>g</sub>), 631 cm<sup>-1</sup> (A<sub>1g</sub>) and 775 cm<sup>-1</sup> (B<sub>2g</sub>)). When the particle size decreases, A<sub>1g</sub> and B<sub>2g</sub> modes of SnO<sub>2</sub> are shifted to lower wavenumbers and E<sub>g</sub> mode is shifted to higher wavenumber<sup>36</sup>. Obtained results have shown that mode at 475 cm<sup>-1</sup> is assigned to translational mode (E<sub>g</sub>) of the oxide. On the other hand, mode

at  $620\text{ cm}^{-1}$  is assigned to symmetric O-Sn-O stretching ( $A_{1g}$ ) and the third mode at  $752\text{ cm}^{-1}$  is assigned to asymmetric O-Sn-O stretching ( $B_{2g}$ )<sup>37</sup>.

The position of  $\text{SnO}_2$  peak in Raman spectrum is dependent of particle size and a fourth vibrational mode ( $B_{1g}$ ) peak appears only to nanomaterials. Thus, in the Raman spectrum the presence of an intense peak centered at  $125\text{ cm}^{-1}$  is associated to non degenerated  $B_{1g}$  mode of  $\text{SnO}_2$  and is assigned to rotation of the oxygen atoms, with all oxygen atoms participating in the vibration at tetragonal unit cell of rutile<sup>36</sup>. All modes and assignments are presented in Table 3.

The effects of particle size and disorder in the material lead to a relaxation of the Raman selection rule, and some modes that are usually inactive in Raman become actives. Furthermore, the peaks at  $242\text{ cm}^{-1}$ ,  $347\text{ cm}^{-1}$ ,  $540\text{ cm}^{-1}$  and  $681\text{ cm}^{-1}$  were assigned to optical phonon modes of  $\text{SnO}_2$ ,  $E_u(1)\text{ TO}$ ,  $E_u(2)\text{ LO}$ ,  $A_{2u}\text{ TO}$  and  $A_{2u}\text{ LO}$  of  $\text{SnO}_2$ , where LO and TO are longitudinal and transverse optical phonons, respectively<sup>34,38-40</sup>.

Peaks at  $1354$  and  $1587\text{ cm}^{-1}$  are termed D and G bands, respectively<sup>41</sup>, and confirm the presence of amorphous carbon

## References

- Umeda J, Kondoh K and Michiura Y. Process parameters optimization in preparing high-purity amorphous silica originated from rice husks. *Materials Transactions*. 2007; 48(12):3095-3100. <http://dx.doi.org/10.2320/matertrans.MK200715>.
- Shen J, Liu X, Zhu S, Zhang H and Tan J. Effects of calcination parameters on the silica phase of original and leached rice husk ash. *Materials Letters*. 2011; 65(8):1179-1183. <http://dx.doi.org/10.1016/j.matlet.2011.01.034>.
- Adam F, Appaturi JN, Khanam Z, Thankappan R and Nawi MAM. Utilization of tin and titanium incorporated rice husk silica nanocomposite as photocatalyst and adsorbent for the removal of methylene blue in aqueous medium. *Applied Surface Science*. 2013; 264:718-726. <http://dx.doi.org/10.1016/j.apsusc.2012.10.106>.
- Gorthy P and Pudukottah M. Production of silicon carbide from rice husks. *Journal of the American Ceramic Society*. 1999; 82(6):1393-1400. <http://dx.doi.org/10.1111/j.1151-2916.1999.tb01929.x>.
- Adam F, Appaturi JN and Iqbal A. The utilization of rice husk silica as a catalyst: review and recent progress. *Catalysis Today*. 2012; 190(1):2-14. <http://dx.doi.org/10.1016/j.cattod.2012.04.056>.
- Adam F and Chua JH. The adsorption of palmytic acid on rice husk ash chemically modified with Al(III) ion using the sol-gel technique. *Journal of Colloid and Interface Science*. 2004; 280(1):55-61. <http://dx.doi.org/10.1016/j.jcis.2004.07.006>. PMID:15476773.
- Gaydhankar TR, Joshi PN, Kalita P and Kumar R. Optimal synthesis parameters and application of Sn-MCM-41 as an efficient heterogeneous catalyst in solvent-free Mukaiyama-type aldol condensation. *Journal of Molecular Catalysis A Chemical*. 2007; 265(1-2):306-315. <http://dx.doi.org/10.1016/j.molcata.2006.10.041>.
- Naskar MK and Chatterjee M. A novel process for the synthesis of lithium aluminum silicate powders from rice husk ash and other water-based precursor materials. *Materials Letters*. 2005; 59(8-9):998-1003. <http://dx.doi.org/10.1016/j.matlet.2004.06.075>.
- Ganesan K, Rajagopal K and Thangavel K. Rice husk ash blended cement: Assessment of optimal level of replacement for

that is typical of the temperature and of the sol-gel route used to obtain the nanocomposite.

## 4. Conclusion

Biogenic  $\text{SiO}_2$  extracted from rice husk and the  $\text{SnO}_2/\text{SiO}_2$  nanocomposite were characterized by XRF, XRD, SEM, FTIR and Raman. The method used in  $\text{SiO}_2$  extraction was efficient to obtain amorphous biogenic  $\text{SiO}_2$  of high purity in nanometer scale.  $\text{SnO}_2/\text{SiO}_2$  nanocomposite behaved as a solid mixture of  $\text{SiO}_2$  of low crystallinity and crystalline  $\text{SnO}_2$ . Therefore, from rice husk is possible to obtain biogenic  $\text{SiO}_2$  of high purity that added to  $\text{SnO}_2$  provide the  $\text{SnO}_2/\text{SiO}_2$  nanocomposite.

## Acknowledgements

The authors acknowledge financial assistance from FAPEAM (Grant # 2985/2012) and the Laboratory of Advanced Optical Spectroscopy (LMEOA/IQ-UNICAMP/FAPESP Grant # 2009/54066-7) for use of Raman equipment.

- strength and permeability properties of concrete. *Construction & Building Materials*. 2008; 22(8):1675-1683. <http://dx.doi.org/10.1016/j.conbuildmat.2007.06.011>.
- Lakshmanan R, Okoli C, Boutonnet M, Jaras S and Rajarao GK. Microemulsion prepared magnetic nanoparticles for phosphate removal: Time efficient studies. *Journal of Environmental Chemical Engineering*. 2014; 2(1):185-189. <http://dx.doi.org/10.1016/j.jece.2013.12.008>.
- Yang W, Gao Z, Wang J, Wang B and Liu L. Hydrothermal synthesis of reduced graphene sheets/ $\text{Fe}_2\text{O}_3$  nanorods composites and their enhanced electrochemical performance for supercapacitors. *Solid State Sciences*. 2013; 20:46-53. <http://dx.doi.org/10.1016/j.solidstatesciences.2013.03.011>.
- Ebrahimi A, Pirouz A, Abdi Y, Azimi S and Mohajerzadeh S. Selective deposition of  $\text{CuO}/\text{SnO}_2$  sol-gel on porous  $\text{SiO}_2$  suitable for the fabrication of MEMS-based  $\text{H}_2\text{S}$  sensors. *Sensors and Actuators. B, Chemical*. 2012; 173:802-810. <http://dx.doi.org/10.1016/j.snb.2012.07.104>.
- Manjula P, Satyanarayana L, Swarnalatha Y and Manorama SV. Raman and MASNMR studies to support the mechanism of low temperature hydrogen sensing by Pd doped mesoporous  $\text{SnO}_2$ . *Sensors and Actuators. B, Chemical*. 2009; 138(1):28-34. <http://dx.doi.org/10.1016/j.snb.2009.02.051>.
- Zhao Y, Liu J, Liu Q, Sun Y, Song D, Yang W, et al. One-step synthesis of  $\text{SnO}_2$  hollow microspheres and its gas sensing properties. *Materials Letters*. 2014; 136:286-288. <http://dx.doi.org/10.1016/j.matlet.2014.08.073>.
- Wang F, Song X, Yao G, Zhao M, Liu R, Xu M, et al. Carbon-coated mesoporous  $\text{SnO}_2$  nanospheres as anode material for lithium ion batteries. *Scripta Materialia*. 2012; 66(8):562-565. <http://dx.doi.org/10.1016/j.scriptamat.2012.01.003>.
- Shimizu K, Katagiri M, Satokawa S and Satsuma A. Sintering-resistant and self-regenerative properties of  $\text{Ag}/\text{SnO}_2$  catalyst for soot oxidation. *Applied Catalysis B: Environmental*. 2011; 108-109:39-46. <http://dx.doi.org/10.1016/j.apcatb.2011.08.003>.
- Dou X, Sabba D, Mathews N, Wong LH, Lam YM and Mhaisalkar S. Hydrothermal Synthesis of High Electron Mobility Zn-doped  $\text{SnO}_2$  Nanoflowers as Photoanode Material for Efficient Dye-Sensitized Solar Cells. *Chemistry of Materials*. 2011; 23(17):3938-3945. <http://dx.doi.org/10.1021/cm201366z>.

18. Feng YS, Zhou SM, Li Y and Zhang LD. Preparation of the SnO<sub>2</sub>/SiO<sub>2</sub> xerogel with a large specific surface area. *Materials Letters*. 2003; 57(16-17):2409-2412. [http://dx.doi.org/10.1016/S0167-577X\(02\)01245-4](http://dx.doi.org/10.1016/S0167-577X(02)01245-4).
19. Granger G, Restoin C, Roy P, Jamier R, Rougier S, Lecomte A, et al. Nanostructured optical fibers in the SiO<sub>2</sub>/SnO<sub>2</sub> system by the sol-gel method. *Materials Letters*. 2014; 120:292-294. <http://dx.doi.org/10.1016/j.matlet.2014.01.104>.
20. An GH and Ahn HJ. Fabrication of SnO<sub>2</sub> and SiO<sub>2</sub> nanoparticle-embedded carbon nanofiber composites via co-electrospinning. *Ceramics International*. 2012; 38(4):3197-3201. <http://dx.doi.org/10.1016/j.ceramint.2011.12.024>.
21. Grieken RV, Martos C, Sánchez MS, Serrano DP, Melero JA, Iglesias J, et al. Synthesis of Sn-silicalite from hydrothermal conversion of SiO<sub>2</sub>-SnO<sub>2</sub> xerogels. *Microporous and Mesoporous Materials*. 2009; 119:176-185.
22. Adam F, Appaturri JN, Thankappan R and Nawi MAM. Silica-tin nanotubes prepared from rice husk ash by sol-gel method: Characterization and its photocatalytic activity. *Applied Surface Science*. 2010; 257(3):811-816. <http://dx.doi.org/10.1016/j.apsusc.2010.07.070>.
23. Lorenzi R, Lauria A, Mochenova N, Chiodini N and Paleari A. Study of the absorption edge of SnO<sub>2</sub> nanoparticles embedded in silica films. *Journal of Non-Crystalline Solids*. 2011; 357(8-9):1888-1891. <http://dx.doi.org/10.1016/j.jnoncrysol.2010.12.045>.
24. Wei TY, Kuo CY, Hsu YJ, Lu SY and Chang YC. Tin oxide nanocrystals embedded in silica aerogel: Photoluminescence and photocatalysis. *Microporous and Mesoporous Materials*. 2008; 112(1-3):580-588. <http://dx.doi.org/10.1016/j.micromeso.2007.10.040>.
25. Zhu Y, Chen J, Li H, Zhu Y and Xu J. Synthesis of mesoporous SnO<sub>2</sub>-SiO<sub>2</sub> composites and their application as quartz crystal microbalance humidity sensor. *Sensors and Actuators. B, Chemical*. 2014; 193:320-325. <http://dx.doi.org/10.1016/j.snb.2013.11.091>.
26. Pechini MP. *Method of preparing lead and alkaline earth titanates and niobates and coating method using the same to form a capacitor*. US 3330697. 1967 July 11.
27. Yalcá N and Sevinç V. Studies on silica obtained from rice husk. *Ceramics International*. 2001; 27:219-224. [http://dx.doi.org/10.1016/S0272-8842\(00\)00068-7](http://dx.doi.org/10.1016/S0272-8842(00)00068-7).
28. Della VP, Hotza D, Junkes JA and Oliveira APN. Estudo comparativo entre sílica obtida por lixívia ácida da casca de arroz e sílica obtida por tratamento térmico da cinza de casca de arroz. *Química Nova*. 2006; 29(6):1175-1179. <http://dx.doi.org/10.1590/S0100-40422006000600005>.
29. Yu X, Tian J, Xie H, Shen H and Wang Q. The integrated production of microbial lipids and bio-SiO<sub>2</sub> from rice husks by an organic electrolytes pretreatment technology. *Bioresource Technology*. 2014; 153:403-407. <http://dx.doi.org/10.1016/j.biortech.2013.12.039>. PMID:24398252.
30. Watari TI, Nakata A, Kiba Y, Torikai T and Yada M. Fabrication of porous SiO<sub>2</sub>/C composite from rice husks. *Journal of the European Ceramic Society*. 2006; 26(4-5):797-801. <http://dx.doi.org/10.1016/j.jeurceramsoc.2005.06.013>.
31. Yang S and Gao L. Facile and surfactant-free route to nanocrystalline mesoporous tin oxide. *Journal of the American Ceramic Society*. 2006; 89(5):1742-1744. <http://dx.doi.org/10.1111/j.1551-2916.2006.00947.x>.
32. Jung HY, Gupta RK, Oh EO, Kim YH and Whang CM. Vibrational spectroscopic studies of sol-gel derived physical and chemical bonded ORMOSILs. *Journal of Non-Crystalline Solids*. 2005; 351(5):372-379. <http://dx.doi.org/10.1016/j.jnoncrysol.2005.01.004>.
33. Li Z, Shen W, Zhang X, Fang L and Zu X. Controllable growth of SnO<sub>2</sub> nanoparticles by citric acid assisted hydrothermal process. *Colloids and Surfaces. A, Physicochemical and Engineering Aspects*. 2008; 327(1-3):17-20. <http://dx.doi.org/10.1016/j.colsurfa.2008.05.043>.
34. Mohamed SH. SnO<sub>2</sub> dendrites-nanowires for optoelectronic and gas sensing applications. *Journal of Alloys and Compounds*. 2012; 510(1):119-124. <http://dx.doi.org/10.1016/j.jallcom.2011.09.006>.
35. Katiyar RS, Dawson P, Hargreave MM and Wilkinson GR. Dynamics of the rutile structure. III. Lattice dynamics, infrared and Raman spectra of SnO<sub>2</sub>. *Journal of Physics. C. Solid State Physics*. 1971; 4(15):2421-2431. <http://dx.doi.org/10.1088/0022-3719/4/15/027>.
36. Diéguez A, Rodríguez AR, Vilà A and Morante JR. The complete Raman spectrum of nanometric SnO[sub 2] particles. *Journal of Applied Physics*. 2001; 90(3):1550-1557. <http://dx.doi.org/10.1063/1.1385573>.
37. Li L. Growth and photoluminescence properties of SnO<sub>2</sub> nanobelts. *Materials Letters*. 2013; 98:146-148. <http://dx.doi.org/10.1016/j.matlet.2013.02.038>.
38. Mendes PG, Moreira ML, Tebcherani SM, Orlandi MO, Andrés J, Li MS, et al. SnO<sub>2</sub> nanocrystals synthesized by microwave-assisted hydrothermal method: towards a relationship between structural and optical properties. *Journal of Nanoparticle Research*. 2012; 14(3):750-762. <http://dx.doi.org/10.1007/s11051-012-0750-7>.
39. Zhou JX, Zhang MS, Hong JM and Yin Z. Raman spectroscopic and photoluminescence study of single-crystalline SnO<sub>2</sub> nanowires. *Solid State Communications*. 2006; 138(5):242-246. <http://dx.doi.org/10.1016/j.ssc.2006.03.007>.
40. Sun SH, Meng GW, Zhang GX, Gao T, Geng BY, Zhang LD, et al. Raman scattering study of rutile SnO<sub>2</sub> nanobelts synthesized by thermal evaporation of Sn powders. *Chemical Physics Letters*. 2003; 376(1-2):103-107. [http://dx.doi.org/10.1016/S0009-2614\(03\)00965-5](http://dx.doi.org/10.1016/S0009-2614(03)00965-5).
41. Faria DLA and Lopes FN. Análise de pinturas rupestres do Abrigo do Janelão (Minas Gerais) por microscopia raman. *Química Nova*. 2011; 34(8):1358-1364. <http://dx.doi.org/10.1590/S0100-40422011000800012>.